Available online at www.sciencedirect.com
SCIENCE DIRECT®
ELSEVIER
Earth and Planetary Science Letters 213 (2003) 417–430
EPSL
www.elsevier.com/locate/epsl

Melt migration in plume–ridge systems

Michael G. Braun *, Robert A. Sohn

Department of Marine Geology and Geophysics, Woods Hole Oceanographic Institution, Woods Hole, MA 02543, USA

Received 7 October 2002; received in revised form 9 March 2003; accepted 5 May 2003

Abstract

We assess the potential for melt migration, separate from solid flow, to accommodate the transport of plume-signature material from off-axis mantle plumes to nearby mid-ocean ridges. We use a boundary-element method to estimate the solid pressures induced by buoyant plume flow, and find that the solid pressure gradients are small compared to melt buoyancy, suggesting that melt streamlines in mantle plumes are essentially vertical. We combine our plume pressure solutions with analytical pressure fields for ridge corner flow and find that the combined plume–ridge pressure field is not sufficient to drive porous flow in the upper mantle over the distances (hundreds of km) observed in many natural systems. We also examine melt transport via porous flow in a melt-rich layer at the base of the lithosphere for plume–ridge systems, and find that melts can traverse plume–ridge offsets of several hundred kilometers in a few hundred thousand years, or less. Our results suggest that plume signatures observed in ridge basalts can be explained by lateral migration of plume melts in a sub-lithospheric channel augmented by solid flow pressure gradients. We apply our models to the Galápagos plume–ridge system and find that melt migration, as opposed to solid flow, provides a means to explain many aspects of the observed chemical anomalies on the Galápagos Spreading Center, including the position of the maximum anomalies due north of the archipelago, the symmetric pattern, and the gradual along-axis gradient.

Keywords: melt migration; plume–ridge interaction; pressure gradients; Galápagos

1. Introduction

Mid-ocean ridges are mobile features that migrate across ocean basins at rates of up to ~50 mm/yr [1–3]. Mantle plumes, in contrast, are believed to be essentially stationary in a global reference frame [4]. Therefore, the two volcanic systems interact when ridges move across hotspots. Lavas associated with mantle plumes (OIBs) and mid-ocean ridges (MORBs) have distinct compositions and isotopic characteristics, which are generally attributed to melting of distinct mantle sources. Ridges are believed to tap a depleted upper mantle, while plume melts are derived from more enriched and isotopically distinct sources [5].

Plume chemical signatures, however, are observed in mid-ocean ridge basalts near hotspots (e.g. [6]), which requires the lateral transport of plume-signature material to the ridge, in some

* Corresponding author. Tel.: +1-508-289-2615; Fax: +1-508-457-2183.
E-mail address: mbraun@whoi.edu (M.G. Braun).

0012-821X/03/$ – see front matter © 2003 Elsevier B.V. All rights reserved.
doi:10.1016/S0012-821X(03)00279-6

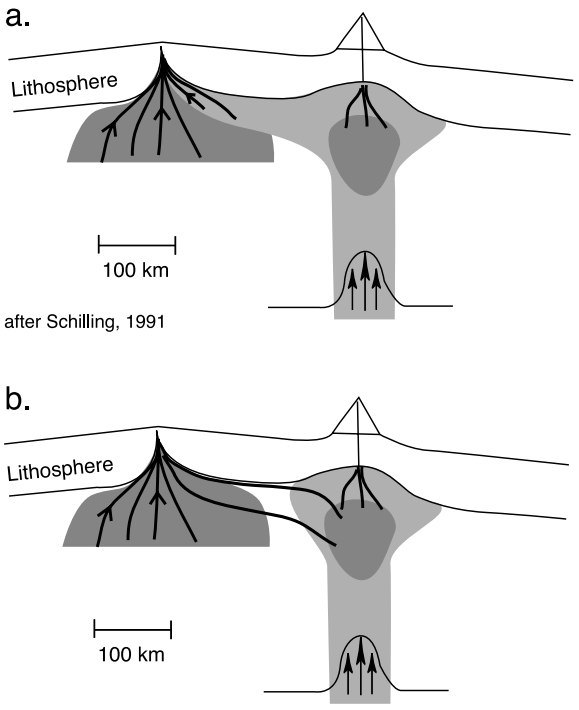

Fig. 1. Two end-member hypotheses to explain plume-signature lavas erupted along spreading centers near hotspots. (a) Solid plume material flows to the ridge and melts, mixing with normal MORB. (b) Plume melts migrate to the ridge independently of the solid.

cases over length scales up to 1000 km. Previous work has largely focused on the transport of solid plume mantle into the melting region beneath a ridge (Fig. 1a). As an alternative, we propose that mass transport is accommodated by porous flow of plume melts to the ridge axis (Fig. 1b).

Two mechanisms have been proposed for the lateral transport of solid plume material toward a ridge axis. Buoyant solid material may flow toward the ridge axis in response to gradients in lithospheric basal topography, possibly focused into a channel eroded by the passing plume. (e.g. [6,7]) Alternatively, plume 'self-spreading' in response to the overlying lithosphere can push solid material towards the ridge, provided the plume volume flux is large compared to the ridge spreading rate (e.g. [8–10]). The relative importance of lithospheric topography and self-spreading on plume flow near ridges is unresolved, but neither mechanism is entirely consistent with the range of geochemical and geophysical observations from plume–ridge systems.

Plume melts may migrate towards a ridge as liquids independent of their solid source material. Lateral melt migration is apparently required to reconcile a broad melting region [11] with a narrow zone of accretion in ridge corner flow systems [12]. While many of the melt focusing mechanisms proposed for ridges (e.g. [13]) would be expected to be equally effective in plume–ridge systems, the hypothesis that plume-signature material migrates to the ridge as melt, rather than solid, has not been formally treated. This is partly attributable to the difficulties associated with fluid dynamic modeling, since similarity principles cannot be exploited to develop analytic expressions for two-phase flow in mantle plumes.

In this study we assess the hypothesis that mass transport between plumes and ridges is accommodated by liquid as opposed to solid flow (Fig. 1), and we place constraints on the nature of melt migration in plume–ridge systems. We focus on two potential mechanisms for melt migration between plumes and ridges: lateral flow in response to solid pressure gradients in the upper mantle and channeled flow beneath an impermeable, sloping lithosphere. We use a boundary-element approach to estimate the pressure field associated with solid plume flow, and find that the pressure gradients are weak compared to melt buoyancy forces, suggesting that melt streamlines in plumes are essentially vertical. However, once melts reach the base of a sloping lithosphere, melt migration through a melt-rich layer may be an effective mechanism for transporting plume signatures large distances (hundreds of kilometers) towards a ridge axis.

2. Pressure field for mantle plume solid flow

Mantle flow in plume systems is driven by the intrinsic buoyancy of the solid plume material as opposed to the motion of overlying tectonic plates. As a result, plume flow fields cannot be calculated analytically by satisfying boundary conditions for coupled differential equations as

has been done for ridges and arcs [14,15], but rather must be solved via numerical methods. We calculate the stream function, velocity, pressure, and pressure gradient fields induced by a plume by modeling it as a buoyant cylinder impinging on the base of a rigid plate (Fig. 2). These calculations expand upon the solution of Ribe and Christensen [16] by including the independent pressure calculation.

The equations governing solid flow in this model balance momentum:

$$-\nabla P + \eta \nabla^2 u + b\delta(x - x^0) = 0 \quad (1)$$

and conserve mass:

$$\nabla \cdot u = 0 \quad (2)$$

subject to the imposed boundary conditions of no slip along the base of the plate and zero velocity far from the buoyancy source. Parameter definitions and their values are listed in Table 1 or defined below. Following Pozrikidis [17], we utilize the Green's function solutions for velocity and pressure, respectively, which have the form:

$$u = \frac{R^2}{8\pi\eta} \int \mathbf{G}(x, x^0) b \mathrm{d}x \quad (3)$$

$$P = \frac{R}{8\pi} \int \Pi(x, x^0) b \mathrm{d}x \quad (4)$$

where R is the radius of the plume, η is the solid viscosity, which is assumed constant, and δ represents the three-dimensional delta function applied to the load b located at position x^0. The Green's functions, $\mathbf{G}$ and $\mathbf{\Pi}$, are calculated using the stokeslet approach of Blake [18] as explicitly described by Pozrikidis ([17], pp. 253–258). Essentially, the force at any position x in the solution domain is the sum of the forces associated with discrete load elements (located at x^0) that comprise the total buoyant load (Fig. 2). Each load element applies a force b which, in the case of buoyancy, acts only in the vertical direction

Table 1
Description of model parameters and values

Variable	Definition	Value
a	Plume aspect ratio	10–25
α	Coefficient of thermal expansion	10^{-6} °C^{-1}
b	Buoyancy force	
C	Geometric constant for permeability	1600
d	Grain size in the mantle	1 cm
ϕ_c	Porosity in sub-lithospheric channel	0.01–0.1
η	Mantle viscosity	10^{19}–10^{22} Pa s
k	Permeability	10^{-12}–10^{-10} m^{-2}
L	Depth of the melting region	70–100 km
λ	Thickness of sub-lithospheric channel	~2 km
M	Melt focusing parameter [14]	0–0.35
P	Pressure field	
R	Plume radius	50–200 km
ρ_{mantle}	Density of the mantle	3300 kg/m^3
ρ_{melt}	Density of basaltic melt	2800 kg/m^3
$\Delta\rho_{mb}$	Density contrast due to melt buoyancy	500 kg/m^3
$\Delta\rho_p$	Density difference between plume and mantle	
ΔT	Plume thermal anomaly	25–300°C
U	Ridge half-spreading rate	10–65 mm/yr
u	Velocity of the solid mantle	
w	Vertical solid upwelling velocity beneath a ridge	
X_0	Maximum degree of melting beneath a ridge	20%
x_{max}	Maximum lateral melt focusing distance	
x,x^0	Spatial coordinates of node points, load elements	

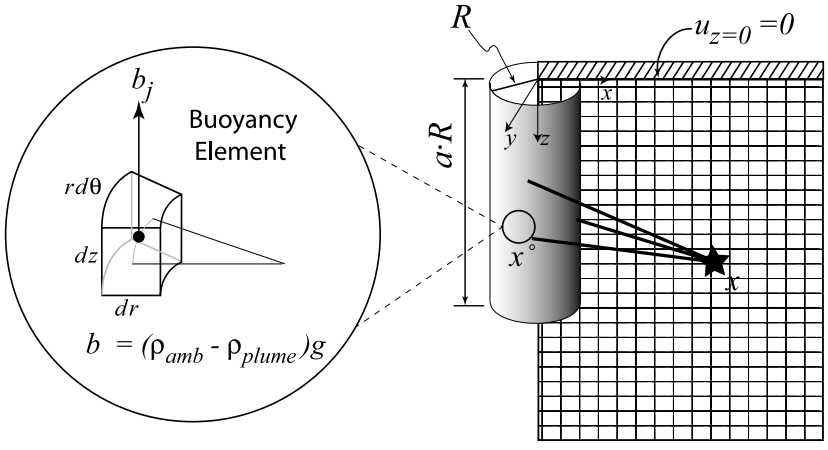

Fig. 2. Cross-section of the axisymmetric solution space for a buoyant cylinder of radius R and aspect ratio a impinging on a stationary rigid lid. Arrows illustrate the influence of multiple load elements, x^0 on the force imposed at a given point, x. Individual load elements (inset) are unit sectors of the cylindrical load with thermally induced buoyancy, b, which acts only vertically.

and in proportion to the density difference, $\Delta\rho_p$, between that element and the ambient mantle. For purely thermal buoyancy, $\Delta\rho_p = \alpha\Delta T$, where α is thermal expansivity and ΔT is the temperature difference between the plume and the ambient mantle. The physical dimensions of each load element are determined by the radius, R, and the aspect ratio, a, of the plume, divided by the total number of load elements (Fig. 2, inset). The number of load elements is sufficiently large such that each can be adequately approximated as a point load for all x in the solution plane. The solid velocities are a function of the plume size, the magnitude of the buoyancy, and the viscosity of the mantle (Eq. 3), while the solid pressures are a function of only plume size and buoyancy (Eq. 4). In contrast to the ridge case, plume solid pressures are independent of viscosity.

We ran our plume flow model with a range of parameterizations corresponding to estimates drawn from geophysical and geochemical investigations of the Galápagos [19–22], Iceland [23–25], and Hawaii [16,26] plumes. In all cases the plume stream function looks similar to that for a spreading ridge, but the velocity and pressure fields are distinctly different as the result of the boundary conditions. Solid velocities are highest along the plume axis and zero at the base of the lithosphere (Fig. 3a). The maximum velocities predicted by the models (Fig. 4a) are comparable to those estimated for natural systems from U-series disequilibria [27] and other numerical models [26,28]. For Hawaii-like ($R = 75$ km, $\Delta T = 200$°C) or Iceland-like ($R = 150$ km, $\Delta T = 250$°C) plumes rising through ambient mantle with a viscosity of 10^{20} Pa s, the maximum upwelling velocities predicted by this model are $\sim$380–1900 mm/yr. For the weaker Galápagos plume ($R = 70$ km, $\Delta T = 100$°C) the maximum upwelling velocity is predicted to be $\sim$90 mm/yr.

The maximum pressures associated with buoyant plume flow are found at the base of the rigid lithosphere and decrease radially away from the plume axis (Fig. 3b). The maximum pressure scales with the total buoyancy and is on the order of tens of megapascals (Fig. 4b). These pressures are consistent with the observed dynamic topography associated with hotspot swells. Assuming all the topography associated with the Hawaiian swell is due to uplift of a 100-km-thick elastic plate by the plume, the pressure required to maintain the observed topography (1300 m over $\sim$1000 km [29]) is of order 10 MPa [30]. Inclusion of viscous restoring forces would increase this pressure estimate further.

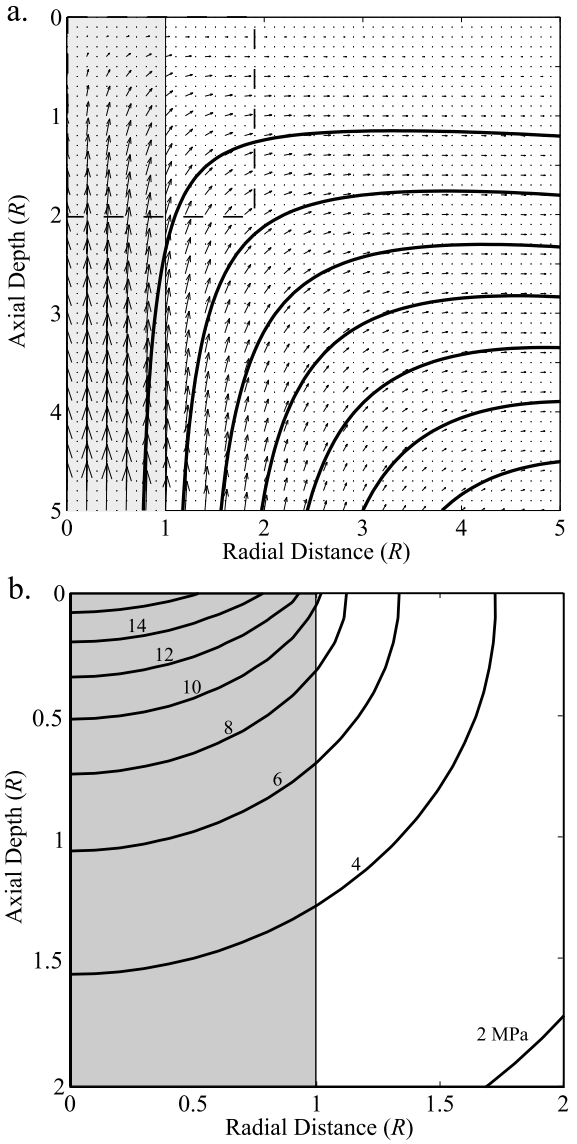

Fig. 3. Model results for a plume ($\Delta T = 200$°C). (a) Velocity vectors and streamlines (solid lines) for solid flow induced by the buoyant plume (shaded rectangle). (b) Pressure field (in MPa) induced by the buoyant plume plotted within the dashed box delineated in (a).

3. Melt migration in plume–ridge systems

3.1. Melt migration in response to solid pressure gradients

Solid mantle flow induces pressure gradients that can drive porous melt migration. The pressure gradients derived solely from buoyancy-driven flow in a plume are directed down and away from the plume axis, decreasing in magnitude

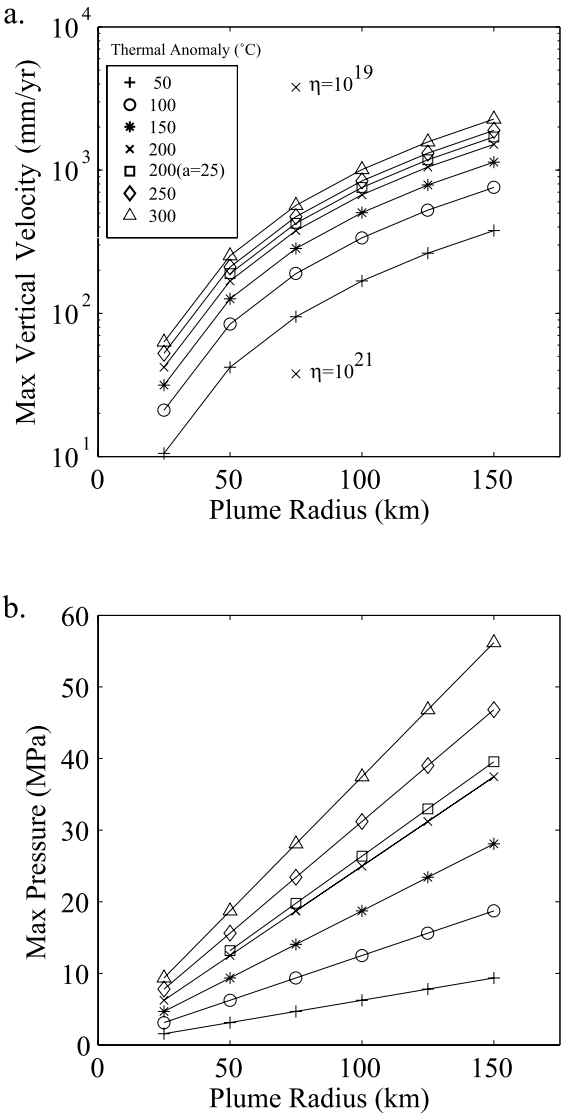

Fig. 4. Maximum upwelling velocity (a) and maximum pressure (b) as a function of plume radius and thermal anomaly (i.e. total buoyancy). For all cases, except where noted, $a = 10$ and $\eta = 10^{20}$ Pa s. The viscosity of the ambient mantle directly affects the upwelling velocity, but has no influence on the pressure field, due to the constant stress boundary conditions, as described in the text. For a constant thermal anomaly, the influence of the depth of origin ($a \times R$) of the plume on velocity and pressure is negligible.

with increasing distance from the center of the plume (Fig. 5a). The magnitude of the pressure gradients scales with buoyancy (Fig. 6), and, in contrast to ridge corner flow, is independent of viscosity. For all realistic combinations of plume size and buoyancy, the pressure gradients induced

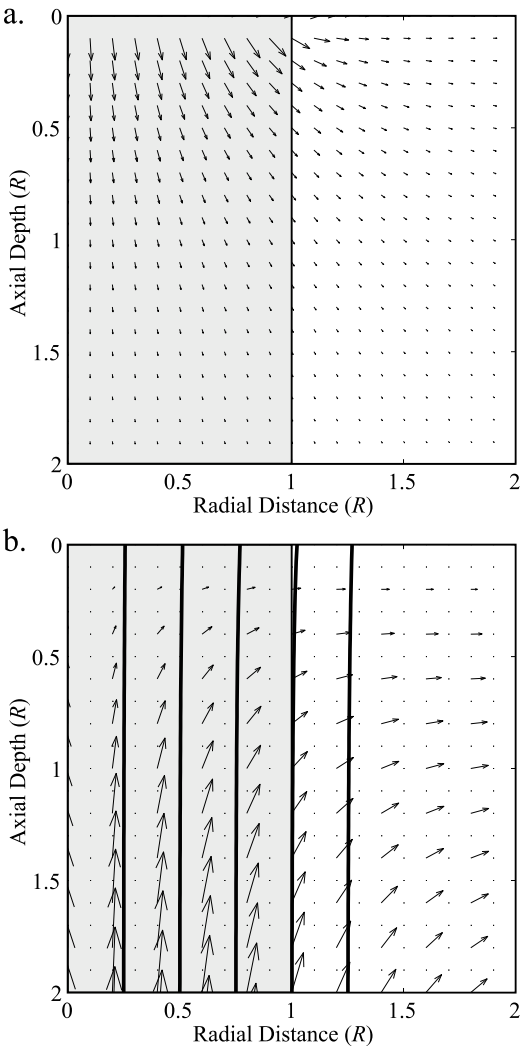

Fig. 5. (a) Pressure gradients induced by solid flow of a plume ($\Delta T = 200$°C) as predicted by the model. Without gravity, melts would be driven down and away from the top of the plume. (b) However, the total pressure gradients, including melt buoyancy, are only weakly influenced by solid flow of the plume, as indicated by the nearly vertical melt streamlines (heavy solid lines). Vectors indicate the solid flow field. The location of the plume is indicated by the shaded rectangle.

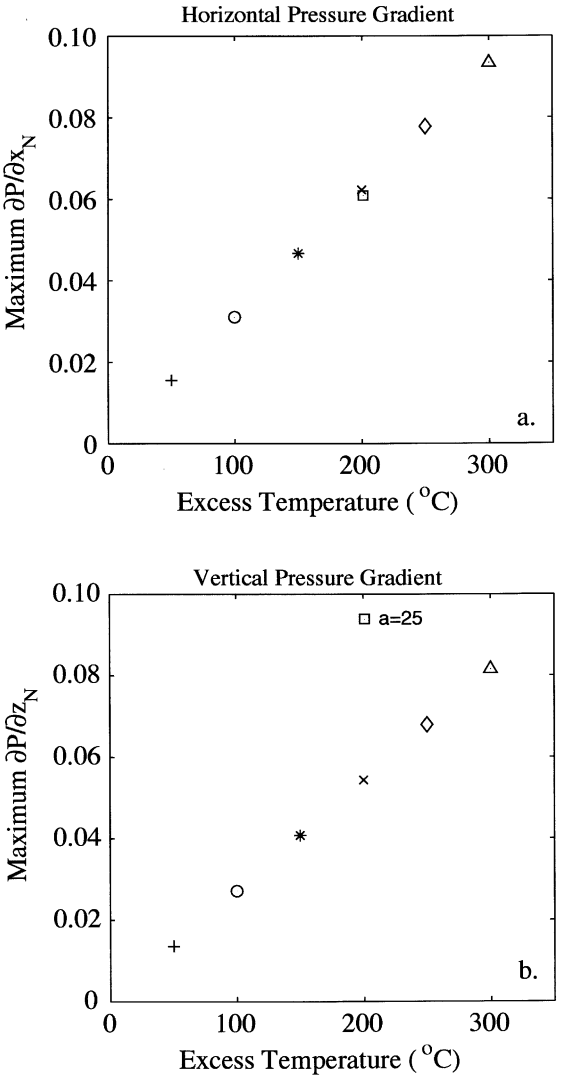

Fig. 6. Maximum (a) radial and (b) vertical pressure gradients (normalized by melt buoyancy, $\Delta\rho_{mb}g$) are strongly dependent upon the thermal anomaly of the plume. Even for the hottest plumes, the pressure gradients are less than 10% of the magnitude of melt buoyancy. All solutions from Fig. 4 are shown here, and the symbols are the same. Both the vertical and horizontal pressure gradients are independent of plume radius and viscosity. The plume aspect ratio affects the vertical pressure gradient, but does not significantly influence lateral melt migration.

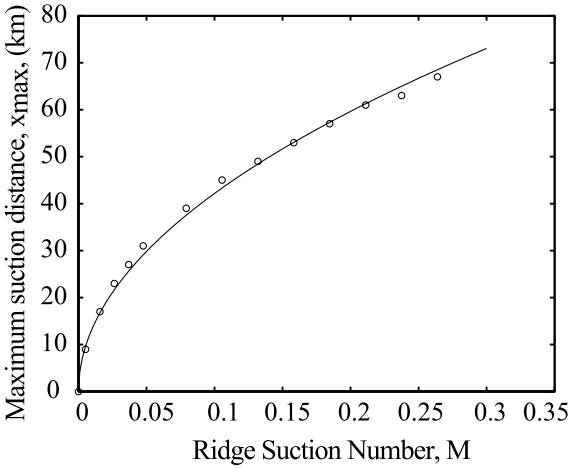

Fig. 7. Maximum lateral melt migration distance versus ridge suction number, M, as defined by Phipps Morgan [14]. Melts generated at a depth of 100 km (plume melting) migrate through the ridge solid flow field in response to buoyancy and solid pressure gradients for a range of M values. Circles represent the maximum lateral offset distance over which these melts were able to migrate to the ridge axis. Straight line is the least-squares best-fit curve to the numerical data.

by solid flow are $<10\%$ of melt buoyancy, $\Delta\rho_{mb}g$, where $\Delta\rho_{mb}$ is the density contrast between melts and the ambient mantle ($\rho_{mantle}-\rho_{melt}$). Thus we find that melt streamlines in plumes are essentially vertical (Fig. 5b).

Our results indicate that any significant lateral melt migration between plumes and ridges in response to solid pressure gradients must be driven by ridge corner flow, with little to no contribution from buoyant plume flow. Divergence of the overlying lithosphere at an oceanic spreading center generates pressure gradients that draw melts towards the ridge axis [14,15]. The magnitude of the lateral pressure gradients in comparison to melt buoyancy can be expressed in terms of the dimensionless ratio $M=4\eta U/\Delta\rho_{mb}gL^2$, where U is the half-spreading rate, η is the mantle shear viscosity, and L is the depth of the melting region [14]. Lateral pressure gradients at ridges are only significant in comparison to melt buoyancy for $M\geq 0.01$, which, for a reasonable range in spreading rates, is possible if η is on the order of 10^{21} Pa s. The shear viscosity of the upper mantle beneath ridges is not precisely known, but values as high as 10^{21} Pa s may be possible in a dehydrated depleted MORB mantle [31].

To investigate the possibility that ridge suction can draw plume melts into the ridge volcanic system, we used the analytical solutions derived by Spiegelman and McKenzie [15] and Phipps Morgan [14] for corner flow beneath a ridge to calculate pressure fields for a range of M values. Using numerical methods to generate melt streamlines, we determined the maximum lateral offset distance over which an off-axis melt could reach the ridge (Fig. 7). Then, using least-squares methods, we derived an empirical expression relating the maximum offset distance, x_{max} (km), to the dimensionless number M:

$$x_{max}=133\sqrt{M} \tag{5}$$

which can be rewritten as:

$$x_{max}=9.7\sqrt{U},\ \text{km} \tag{6}$$

(U, mm/yr) if $\eta=10^{21}$ Pa s, $L=70$ km, and $\Delta\rho_{mb}=500$ kg/m^3. The fastest half-spreading rates along the global mid-ocean ridge system are 50–60 mm/yr for the East Pacific Rise, which imply a maximum lateral melt migration distance of $\sim$65 km. Our results thus suggest that lateral melt migration from a plume to a ridge in response to solid pressure gradients is only possible for plume–ridge offset distances less than 65 km.

To further illustrate this point, we estimate the solid flow pressure gradients in a plume–ridge system using parameters consistent with the Galápagos region (Fig. 8). Streamlines for plume-derived melts do not reach the ridge axis, but rather intersect the lithosphere at a minimum distance of $\sim$50 km from the ridge axis.

3.2. *Lateral melt migration beneath an impermeable lithospheric lid*

To first order, the thermal lithosphere represents an impermeable lid that impedes the vertical flow of melts to a position of neutral buoyancy in the crust. Because the lithosphere at a spreading center thickens as it cools with time, the impermeable lid should slope upwards towards the mid-ocean ridge axis. Thus, buoyant melts that accu-

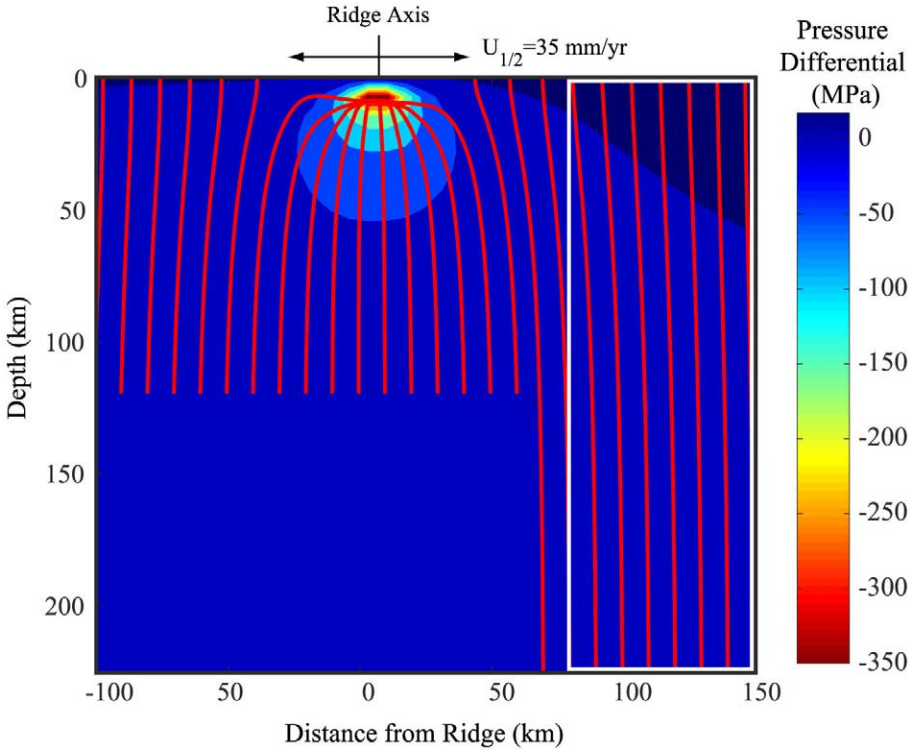

Fig. 8. Combined pressure field and melt flow streamlines for the Galápagos plume–ridge system. The total pressure field was calculated by combining our model for plume-induced pressure field ($\Delta T = 200$, $R = 70$, $a = 10$) with the Spiegelman and McKenzie [15] and Phipps-Morgan [14] models for corner flow pressure field ($U = 29$ mm/yr, $\eta = 10^{21}$ Pa s) at an offset distance of 200 km. Color contours represent the pressure relative to the ambient mantle as a result of solid flow. Negative differential pressures indicate ridge suction; positive differential pressures (dark blue) are the result of the buoyant plume (white rectangle). Melts generated within and around the plume are deflected toward the ridge, but do not reach the ridge axis, as shown by the red streamlines.

mulate beneath the lithosphere would be expected to migrate laterally towards the ridge axis.

Following the analysis of Sparks and Parmentier [32], we assume melt flow toward the ridge axis occurs along the base of the lithosphere in a narrow decompacting layer with an impermeable upper boundary and melt addition from the upwelling mantle below. Melt flow in the conduit is driven by the component of melt buoyancy resolved on the sloping base of the lithosphere and the gradient in non-hydrostatic pressures along the layer (i.e. lateral variations in the decompaction rate). The decompaction term is small relative to the buoyancy term. By assuming all the melt originates at the plume, rather than incrementally added along the channel (as in the ridge case), the porosity in the channel can be held constant, and we can simplify the expression for the lateral pressure gradient in the sub-lithospheric channel to:

$$\partial P/\partial x = (1-\phi_c)\Delta\rho \sin\theta \tag{7}$$

where ϕ_c is the porosity in the channel and θ is slope of the base of the conductively cooling lithosphere at some distance, x, away from the ridge axis. The thickness of the melt-rich layer, λ, is set by the length scale for decompaction, $\lambda = (\eta w X_0/\Delta\rho_{mb} g)^{1/2}$, where w is the solid upwelling rate proportional to U at a given distance from the ridge axis, and X_0 is the maximum degree of melting.

Assuming a mantle viscosity of 10^{21} Pa s, a half-spreading rate of 35 mm/yr, a maximum degree of melting of 20%, a channel porosity of 5%,

and a density difference between the mantle and melt of 500 kg/m^3, this high-porosity layer would have an average thickness of approximately 2 km, increasing towards the axis. The predicted channel thickness is ~10 times larger than that used in the Sparks and Parmentier [32] analysis, primarily because we have assumed a higher mantle viscosity. The predicted channel height, however, is comparable to the thickness of some crust–mantle transition zone dunites in the Oman ophiolite, which were formed in part by melts accumulated at the base of the crust [33]. The predicted pressure gradients driving melt transport in the channel are 10–20% of melt buoyancy at large distances from the ridge axis and rapidly increase approaching the ridge axis (Fig. 9).

Using the calculated lateral pressure gradients in the sub-lithospheric conduit, we estimate the Darcy transport time for off-axis melts to reach the ridge axis. For porous flow through a slowly moving matrix, the melt velocity toward the ridge axis is defined as:

$$v = \frac{k}{\phi_c \eta_{melt}} \frac{\partial P}{\partial x} - U \quad (8)$$

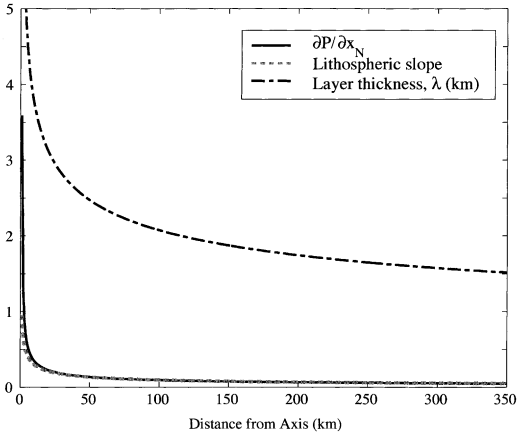

Fig. 9. Melt migration along a decompacted, high-porosity channel of thickness λ (in km), at the base of the lithosphere. As the slope of the base of the lithosphere increases toward the ridge axis as the result of conductive cooling, the component of melt buoyancy, $\partial P/\partial x_N$ (normalized by the magnitude of melt buoyancy, $\Delta\rho_{mb}g$) resolved along the base of the plate also increases. The thickness of the melt-rich layer also increases as melts are continually added from below.

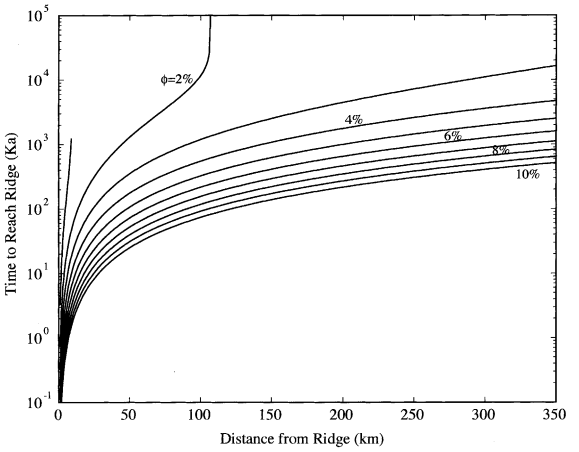

Fig. 10. The time for melts to reach the ridge axis by Darcy flow in a high-porosity conduit along the base of the lithosphere. Melts must travel to the ridge faster than the plate is moving away. For the plate velocity of 35 mm/yr used in this plot, melts can migrate hundreds of kilometers to the rise axis provided the channel porosity is ≥3%.

where the permeability, k, of the conduit is a nonlinear function of its porosity, ϕ_c. Assuming the porous matrix is composed of tetrakaidecahedral grains with a characteristic diameter, d, the permeability can be expressed as:

$$k = \frac{\phi_c^2 d^2}{1600} \quad (9)$$

[34]. For layer porosities of 2–10% and a plate velocity, U, of 35 mm/yr, melts with a viscosity of 10 Pa s could reach the ridge axis from as far as 150 km in less than 200 ka. For layer porosities less than ~2%, the permeability is too small, and melts cannot migrate faster than the plate is moving away from the ridge (Fig. 10). Seismic refraction data are consistent with upper mantle porosities immediately below the crust of 3–12% (e.g. [35]), which is also consistent with estimates for vertical melt channels beneath mid-ocean ridges based on geochemical data [13] and field observations [36]. Some of the melts in this channel freeze due to conductive cooling of the lithosphere [37,38], but this effect is likely reduced in plume–ridge systems where the excess melt flux and additional heat supplied by the plume may

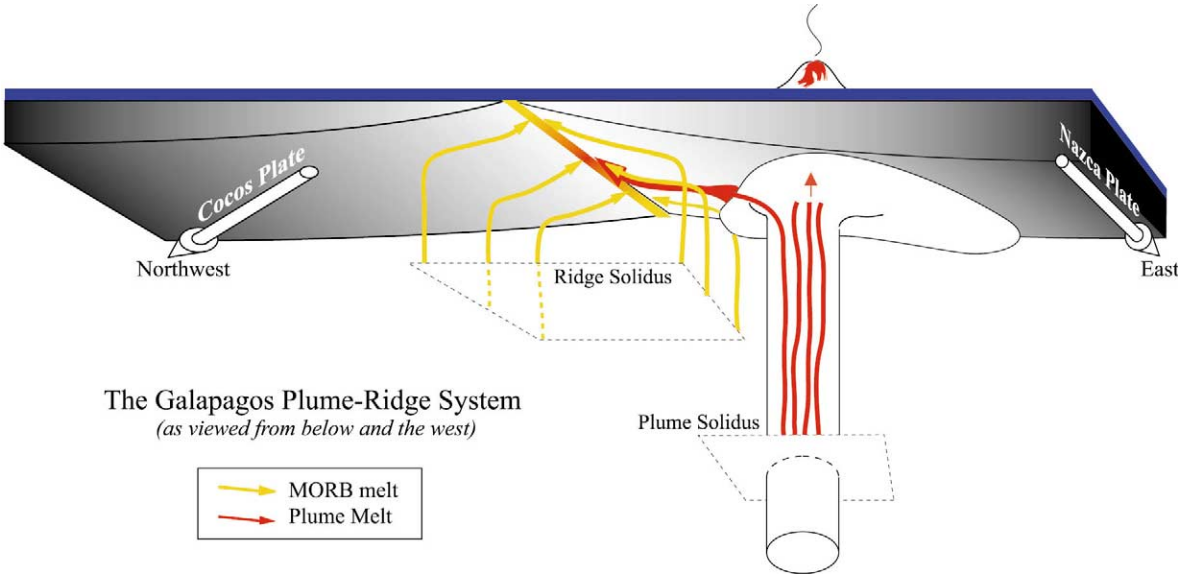

Fig. 11. The Galápagos plume–ridge system as viewed from below and to the west. Solid plume material, rising beneath the Nazca plate, impinges on the base of the lithosphere and is dragged east by the plate, spreading out laterally. While the majority of plume-derived melts (red lines) feed the overlying volcanoes, some melts migrate laterally along the base of the plate to the ridge where they mix with MORB melts (orange lines).

allow igneous temperatures to be sustained over greater portions of the channel.

4. Discussion

4.1. Character of melt migration in plume–ridge systems

Our model results suggest that the lateral pressure gradients induced by solid flow in plume–ridge systems are not large enough to drive lateral melt migration over the length scales (hundreds of kilometers) observed in natural systems (e.g. [39–41]). Channeled melt flow in a high-porosity conduit at the base of the lithosphere, however, appears to provide a feasible mechanism for mass transport between an off-axis plume and a nearby ridge. In principle, large lateral distances can be traversed provided temperatures within the melt channel remain above the solidus and the melt migration velocity is greater than the plate speed relative to the plume. Melts migrating along the base of the lithosphere are capable of reaching the ridge axis from distances of several hundred kilometers in a few hundred thousand years.

4.2. The Galápagos plume–ridge system

To illustrate our results we apply our melt migration models to the relatively well-characterized Galápagos plume–ridge system. Basalt lavas along the Galápagos Spreading Center (GSC) exhibit systematic compositional variations in large-ion lithophile elements and long-lived radiogenic isotopes in the vicinity of the archipelago[42], which appears to result from mixing with Galápagos plume material. The motions of the Cocos and Nazca plates in the hotspot reference frame are 65 mm/yr along 058° and 35 mm/yr along 091°, respectively [43], and as a result the GSC is migrating NE at a rate of ~45 mm/yr along 038°. Thus the plate kinematics differ substantially from the paradigm of two-dimensional, symmetric ridge corner flow since the Nazca plate is moving essentially parallel to the GSC (Fig. 11).

Our model results suggest that solid pressure gradients for the combined plume–ridge system

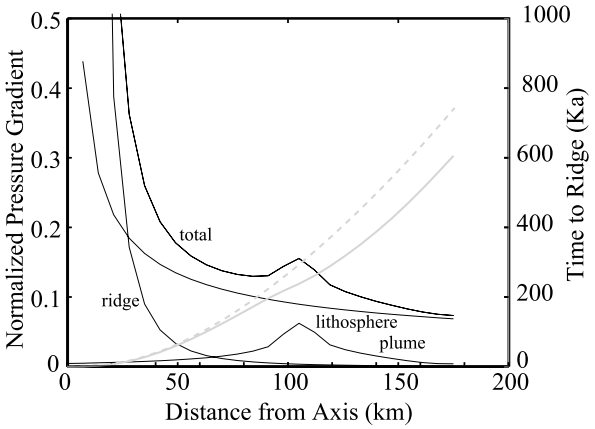

Fig. 12. Lateral pressure gradients (black lines) for melt flow along a high-porosity channel at the base of the plate for the Galápagos plume–ridge system normalized to melt buoyancy. The total pressure gradient is dominated by the solid flow pressure gradients associated with corner flow near the ridge axis. However, farther from the axis (>50 km) the effect of lithospheric slope begins to dominate. Solid plume flow may contribute to pressure gradients in the channel, with a maximum effect at the edge of the buoyant plume. Assuming a channel porosity of 5%, the Darcy transport time of plume melts to the rise axis is on the order of 300 ka without any contribution from the plume (dashed gray line). The migration time may decrease by as much as 135 ka if the plume effects are included (solid gray line).

are insufficient to draw plume melts to the ridge axis (Fig. 8). The pressure gradients may, however, contribute to melt transport along the base of the plate since plume-induced pressures are greatest in this region. The combined effects of lithospheric slope and solid flow pressure gradients at the base of the plate are shown in Fig. 12. The lateral gradients have been normalized by the magnitude of vertical melt buoyancy ($\Delta\rho_{mb}g$) to illustrate the influence of each component on melt migration. Plume flow nearly doubles the total lateral pressure gradient where the effects of lithospheric slope and ridge suction are small far from the ridge axis. This increase in total driving force at the edge of the plume decreases the time required for melts to reach the Galápagos ridge axis by as much as 135 ka and may aid in the expulsion of plume-signature melts into the sub-lithospheric channel and subsequently to the ridge axis. At a distance of 50 km, where the plume melt streamlines reach the base of the lithosphere (Fig. 8), the total pressure gradient has increased to nearly 20% of the magnitude of melt buoyancy, and the migration time to the ridge is less than 100 ka.

We have considered the possibility that mass transport is accommodated by porous melt flow. For comparison, we assess the alternative hypothesis that mass transport is accommodated by solid flow of plume material, in the context of the Galápagos plume–ridge system. Previous work has considered two mechanisms for transporting plume solids to the ridge, buoyant flow along the base of a sloping or channeled lithosphere [8,44] and lateral spreading associated with plume material impinging on the base of the lithosphere [9,10]. If lateral transport between a plume and ridge is accommodated via solid flow, then the plume must be either thin and hot (buoyant flow along base of lithosphere dominates) or wide and with a relatively small thermal anomaly (spreading from large plume volume flux dominates). Ito et al. [10] argued for a wide and relatively cold plume at the Galápagos on the basis of their modeling, but there are some difficulties reconciling this concept with geochemical anomalies in basalts along the GSC. If plume volume fluxes are sufficient to drive plume source material a few hundreds of kilometers to an adjacent ridge, then the solid plume material essentially floods the upper mantle, and mixing between MORB and OIB end-members is limited to a small region at the edge of the solid plume material (see figure 14 of Ito et al. [10]). This prediction contrasts with

observations of gradual along-strike geochemical gradients along plume-influenced ridges that peak with compositions indicative of proportional mixtures between plume (OIB) and MORB end-members [6].

In addition, solid flow models have not incorporated the three-dimensional nature of absolute plate motions (i.e. relative motion between the ridge and the plume) in the Galápagos region. In a relative sense, solid plume material should be advected eastward by the motion of the Nazca plate, which is consistent with the bathymetric swell and the spatial distribution of basalt compositions in the archipelago [19]. Thus, the contribution of solid plume material to basalt chemistry would be expected to be greatest on the GSC east of the archipelago. However, the maximum influence of plume-signature material on basalt composition is observed directly north of the inferred plume center [20,39].

Melt migration in a sub-lithospheric channel provides a means to reconcile many aspects of the geochemical and geophysical data from the Galápagos with fluid dynamics models. For channel porosities greater than $\sim$3%, the lateral melt migration velocity is significantly larger than the plate velocity (as indicated by the nearly horizontal curves in Fig. 10). Plume melts will thus follow the gradient in the lithospheric slope and migrate north to the rise axis, as opposed to being advected east with the plume solid in response to the overlying plate motion (Fig. 11). The melt migration model therefore matches the geochemical observations by predicting a symmetric chemical anomaly on the rise axis with a maximum value directly north of the archipelago. In addition, the buoyancy driving lateral mass transport in a melt migration model, unlike solid flow models, is not a function of solid plume temperature, nor volume flux. As a result, plume material can be transported to the rise axis without invoking excessively large solid plume volume fluxes or temperature anomalies, which has proven to be difficult with solid flow transport models [8,10]. In the melt migration transport model the solid plume temperature and volume flux control the mixing proportions of plume and MORB end-members at the rise axis, along with the magnitude of crustal thickness anomalies. In principle these parameters could be estimated by applying melting models to fluid dynamics models of solid and melt flow, and this may prove to be a fruitful area of research in the future.

In the melt migration model the widths of the along-strike gradients in ridge basalt composition at the GSC are related to the size of the plume and sub-lithospheric topography. Melt production in the plume is proportional to the upwelling velocity and is therefore largely confined to the vertical plume stem [16], implying that the volume flux of plume melts is greatest at the center of the plume and decreases radially outward. The flux of plume melts to the ridge should therefore correlate with the plume vertical velocity profile projected along flow lines to the ridge axis, and the rise axis basalts should have compositions that reflect the local ratio of plume and ridge melt fluxes. We note that the 91°W fracture zone at the GSC, although a prominent feature at the surface, would not be expected to exert much influence on melt migration from the plume to the ridge. Gravity modeling indicates that the base of the lithosphere has only a small offset across the discontinuity from west to east ($\sim$10 km) compared to the ridgeward change in thickness related to age ($\sim$45 km) [45]. The symmetrical nature of the geochemical anomaly about the fracture zone supports this assertion.

We have used simple models to demonstrate that melt flow is potentially an important aspect of plume–ridge interactions, but we have stopped well short of modeling two-phase flow in plume–ridge systems. Development of more advanced numerical models simultaneously incorporating both solid and liquid flow (and their rheological interactions) are clearly needed, as is a treatment of the implications of the melt migration model for basalt geochemistry. Comparison of such models with geophysical and geochemical data from natural plume–ridge systems should provide a means to constrain parameters such as plume volume flux, melt flux, and temperature, and to determine the extent to which geochemical anomalies observed in plume–ridge systems are the result of solid vs. liquid flow.

Acknowledgements

This research grew out of discussions during the 2001 WHOI Geodynamics seminar series on plume–ridge interactions. We are grateful to Neil Ribe for providing critical input, including computer code, and to Chris Small, Marc Spiegelman, Peter Kelemen, and Matthew Jull for insightful discussions of plate kinematics and mantle dynamics. This manuscript benefited from thoughtful reviews by Dennis Geist and Jean-Guy Schilling. This work was sponsored in part by the WHOI Office of Academic Programs.*[BOYLE]*

References

[1] W.J. Morgan, Rises, trenches, great faults, and crustal blocks, J. Geophys. Res. 73 (1968) 1959–1982.
[2] C. Small, L. Danyushevsky, A plate kinematic explanation for mid-oceanic ridge depth discontinuities, Geology 31 (2003) 399–402.
[3] S. Stein, H.J. Melosh, J.B. Minster, Ridge migration and asymmetric sea-floor spreading, Earth Planet. Sci. Lett. 36 (1977) 51–62.
[4] W.J. Morgan, Plate motions and deep mantle convection, studies in earth and space sciences, Mem. Geol. Soc. Am. 132 (1972) 7–22.
[5] S.R. Hart, A. Zindler, W.R.E. Peltier, Constraints on the nature and development of chemical heterogeneities in the mantle, Fluid Mech. Astrophys. Geophys. 4 (1989) 261–387.
[6] J.-G. Schilling, Upper mantle heterogeneities and dynamics, Nature 314 (1985) 62–67.
[7] W.J. Morgan, Rodriguez, Darwin, Amsterdam, ..., a second type of hotspot island, J. Geophys. Res. 83 (1978) 5355–5360.
[8] C. Kincaid, J.-G. Schilling, C. Gable, The dynamics of off-axis plume–ridge interaction in the uppermost mantle, Earth Planet. Sci. Lett. 137 (1996) 29–43.
[9] N.M. Ribe, W.L. Delattre, The dynamics of plume–ridge interaction-III, the effects of ridge migration, Geophys. J. Int. 133 (1998) 511–518.
[10] G. Ito, J. Lin, C.W. Gable, Interaction of mantle plumes and migrating mid-ocean ridges; implications for the Galápagos plume–ridge system, J. Geophys. Res. 102 (1997) 403–415.
[11] D.W. Forsyth, D.S. Scheirer, S.C. Webb, L.M. Dorman, J.A. Orcutt, A.J. Harding, D.K. Blackman, J.P. Morgan, R.S. Detrick, Y. Shen, C.J. Wolfe, J.P. Canales, D.R. Toomey, A.F. Sheehan, S.C. Solomon, W.S.D. Wilcock, Imaging the deep seismic structure beneath a mid-ocean ridge: The MELT experiment, Science 280 (1998) 1215–1218.
[12] E.E. Vera, J.C. Mutter, P. Buhl, A.A. Orcutt, A.J. Harding, M.E. Kappus, R.S. Detrick, T.M. Brocher, The structure of 0- to 0.2-My-old crust at 9 N on the East Pacific Rise from expanded spread profiles, J. Geophys. Res. 95 (1990) 15,529–15,556.
[13] P.B. Kelemen, G. Hirth, N. Shimizu, M. Spiegelman, H.J.B. Dick, A review of melt migration processes in the adiabatically upwelling mantle beneath spreading ridges, Phil. Trans. R. Soc. Lond. A 355 (1997) 283–318.
[14] J. PhippsMorgan, Melt migration beneath mid-ocean spreading centers, Geophys. Res. Lett. 14 (1987) 1238–1241.
[15] M. Spiegelman, D. McKenzie, Simple 2-D models for melt extraction at mid-ocean ridges and island arcs, Earth Planet. Sci. Lett. 83 (1987) 137–152.
[16] N.M. Ribe, U.R. Christensen, The dynamical origin of Hawaiian volcanism, Earth Planet. Sci. Lett. 171 (1999) 517–531.
[17] C. Pozrikidis, Introduction to Theoretical and Computational Fluid Dynamics, Oxford University Press, New York, 1997, 675 pp.
[18] J.R. Blake, A note for the image system for a Stokeslet in a no-slip boundary, Proc. Camb. Phil. Soc. 79 (1971) 303–310.
[19] W.M. White, A.R. McBirney, R.A. Duncan, Petrology and geochemistry of the Galápagos islands: Portrait of a pathological mantle plume, J. Geophys. Res. 98 (1993) 19,533–19,563.
[20] M.D. Kurz, D. Geist, Dynamics of the Galápagos hotspot from helium isotope geochemistry, Geochim. Cosmochim. Acta 63 (1999) 4139–4156.
[21] J.P. Canales, G. Ito, R.S. Detrick, J. Sinton, Crustal thickness along the western Galápagos spreading center and the compensation of the Galápagos hotspot swell, Earth Planet. Sci. Lett. 203 (2002) 311–327.
[22] D.R. Toomey, E.E.E. HooftToomey, S.C. Solomon, D.E. James, M.L. Hall, Upper mantle structure beneath the Galápagos archipelago from body wave data, EOS Trans. AGU 82 (2001) 1205.
[23] C.J. Wolfe, I.T. Bjarnason, J.C. VanDecar, S.C. Solomon, Seismic structure of the Iceland mantle plume, Nature 385 (1997) 245–247.
[24] Y. Shen, S. Solomon, I. Bjarnason, C. Wolfe, Seismic evidence for a lower mantle origin of the Iceland plume, Nature 395 (1998) 62–65.
[25] K. Breddam, M.D. Kurz, M. Storey, Mapping out the conduit of the Iceland mantle plume with helium isotopes, Earth Planet. Sci. Lett. 176 (2000) 45–55.
[26] S. Watson, D. McKenzie, Melt generation by plumes; a study of Hawaiian volcanism, J. Petrol. 32 (1991) 501–537.
[27] K.W. Sims, D.J. DePaolo, M.T. Murrell, W.S. Baldridge, S. Goldstein, D. Clague, M. Jull, Porosity of the melting zone and variations in the solid mantle upwelling rate beneath Hawaii; inferences from ^{238}U-^{230}Th-^{226}Ra and ^{235}U-^{231}Pa disequilibria, Geochim. Cosmochim. Acta 63 (1999) 4119–4138.

[28] E.H. Hauri, J.A. Whitehead, S.R. Hart, Fluid dynamic and geochemical aspects of entrainment in mantle plumes, J. Geophys. Res. 99 (1994) 24,275–24,300.
[29] P. Wessel, Observational constraints on models of the Hawaiian hot spot swell, J. Geophys. Res. 98 (1993) 16,095–16,104.
[30] D. Turcotte, G. Schubert, Geodynamics: Applications of Continuum Mechanics to Geological Problems, Wiley, New York, 1983, 450 pp.
[31] M.G. Braun, G. Hirth, E.M. Parmentier, The effects of deep damp melting on mantle flow and melt generation beneath mid-ocean ridges, Earth Planet. Sci. Lett. 176 (2000) 339–356.
[32] D.W. Sparks, E.M. Parmentier, Melt extraction from the mantle beneath spreading centers, Earth Planet. Sci. Lett. 105 (1991) 368–377.
[33] F. Boudier, A. Nicolas, Nature of the Moho transition zone in the Oman ophiolite, J. Petrol. 36 (1995) 777–796.
[34] N. von Bargen, H.S. Waff, Permeablilities, interfacial areas and curvatures of partially molten systems: results of numerical computations of equilibrium microstructures, J. Geophys. Res. 91 (1986) 9261–9276.
[35] R.A. Dunn, D.R. Toomey, S.C. Solomon, Three-dimensional seismic structure and physical properties of the crust and shallow mantle beneath the East Pacific Rise at 9°30′N, J. Geophys. Res. 105 (2000) 23,537–23,555.
[36] M.G. Braun, P.B. Kelemen, Dunite distribution in the Oman Ophiolite: Implications for melt flux through porous dunite conduits, Geochem. Geophys. Geosyst. 3 (11) (2002) 8603, doi: 10.1029/2001GC000289.
[37] M. Spiegelman, Flow in deformable porous media. Part 1 – Simple analysis, J. Fluid Mech. 247 (1993) 17–38.
[38] A. Ghods, J. Arkani-Hamed, Melt migration beneath mid-ocean ridges, Geophys. J. Int. 140 (2000) 687–697.
[39] S.P. Verma, J.-G. Schilling, D.G. Waggoner, Neodymium isotopic evidence for Galápagos hotspot-spreading centre system evolution, Nature 306 (1983) 654–657.
[40] J.-G. Schilling, Geochemical, isotopic variation along the Mid-Atlantic Ridge axis from 79 degrees N to 0 degrees N, The western North Atlantic region, in: The Geology of North America, 1986, pp. 137–156.
[41] J. Douglass, J.-G. Schilling, D. Fontignie, Plume–ridge interactions of the Discovery and Shona mantle plumes with the southern Mid-Atlantic Ridge (40 degrees-55 degrees S), J. Geophys. Res. 104 (1999) 2941–2962.
[42] J.-G. Schilling, R.H. Kingsley, J.D. Devine, Galápagos hot spot-spreading center system; 1, Spatial petrological and geochemical variations (83W-101W), J. Geophys. Res. 87 (1982) 5593–5610.
[43] A.E. Gripp, R.G. Gordon, Current plate velocities relative to the hotspots incorporating the NUVEL-1 global plate motion model, Geophys. Res. Lett. 17 (1990) 1109–1112.
[44] J.-G. Schilling, Fluxes and excess temperatures of mantle plumes inferred from their interaction with migrating mid-ocean ridges, Nature 352 (1991) 397–403.
[45] M.A. Feighner, M.A. Richards, Lithospheric structure and compensations mechanisms of the Galápagos Archipelago, J. Geophys. Res. 99 (1994) 6711–6729.